Acta Oceanol. Sin., 2017, Vol. 36, No. 8, P. 84–93
DOI: 10.1007/s13131-017-1019-x
http://www.hyxb.org.cn
E-mail: hyxbe@263.net

Thermodynamic model of melt pond and its application during summer of 2010 in the central Arctic Ocean

ZHANG Shugang[1, 3*], BIAN Lingen[2], ZHAO Jinping[3], LI Min[1], CHEN Shizhe[1], JIAO Yutian[3], CHEN Ping[3]

[1] Shandong Provincial Key Laboratory of Ocean Environmental Monitoring Technology, Institute of Oceanographic Instrumentation, Shandong Academy of Sciences, Qingdao 266100, China

[2] Chinese Academy of Meteorological Sciences, Beijing 100081, China

[3] Key Laboratory of Physical Oceanography of Ministry of Education, Ocean University of China, Qingdao 266100, China

Received 19 February 2016; accepted 26 May 2016

Abstract

A one-dimensional thermodynamic model of melt pond is established in this paper. The observation data measured in the summer of 2010 by the Chinese National Arctic Research Expedition (CHINARE-2010) are used to partially parameterize equations and to validate results of the model. About 85% of the incident solar radiation passed through the melt pond surface, and some of it was released in the form of sensible and latent heat. However, the released energy was very little (about 15%), compared to the incident solar radiation. More than 58.6% of the incident energy was absorbed by melt pond water, which caused pond-covered ice melting and variation of pond water temperature. The simulated temperature of melt pond had a diurnal variation and its value ranged between 0.0°C and 0.3°C. The melting rate of upper pond-covered ice is estimated to be around two times faster than snow-covered ice. At same time, the change of melting rate was relatively quick for pond depth less than 0.4 m, while the melting rate kept relatively constant (about 1.0 cm/d) for pond depth greater than 0.4 m.

Key words: Arctic Ocean, melt pond, thermodynamic process, melting rate

Citation: Zhang Shugang, Bian Lingen, Zhao Jinping, Li Min, Chen Shizhe, Jiao Yutian, Chen Ping. 2017. Thermodynamic model of melt pond and its application during summer of 2010 in the central Arctic Ocean. Acta Oceanologica Sinica, 36(8): 84–93, doi: 10.1007/s13131-017-1019-x

1 Introduction

Melt ponds, which include the first- and multi-year ice, are a persistent feature of sea ice in summer. Melt ponds in the Arctic appear at the end of May, and cover a significant portion of the sea ice surface by mid June; the ponds widen and deepen in June and July (sometimes melt passes through the entire ice layer), and begin to refreeze at the end of August or early September (Fetterer and Untersteiner, 1998). Aerial data show that the ponds' percentage quickly increases in mid July and could exceed 20% in early August (Perovich et al., 2002). Toward early September, melt ponds may cover as much as 50% of the sea ice surface (Flocco et al., 2010; Landy et al., 2014). Melt ponds influence the energy and mass balance of sea ice through the albedo-feedback mechanism, can affect the salt and heat budgets of the ocean mixed layer, and alter the optical and physical properties of sea ice (Ebert and Curry, 1993; Eicken et al., 1996).

An important role of melt ponds is altering the albedo of summer sea ice with a lower albedo than sea ice. The albedo of ice ranges from 0.39 to 0.84, whereas the albedo of a melt pond ranges from 0.1 to 0.5 (Grenfell and Maykut, 1977; Fetterer and Untersteiner, 1988). This albedo difference strengthens the melting of pond-covered ice, generating a positive feedback mechanism for sea ice melting (Schröder et al., 2014). Some study suggested that the melting speed of pond-covered ice was estimated to be between 2 and 3 times faster than that of bare ice (Fetterer and Untersteiner, 1998). Melt ponds absorb more solar radiation than sea ice, the additionally acquired solar radiation would warm the pond and cause further melting at the base and sides of the pond; thus, bare ice melts lower than pond-covered ice (Zhang et al., 2014).

There was no pond parameterization in early sea-ice thermodynamic models (Maykut and Untersteiner, 1971; Semtner, 1976). Mellor and Kantha (1989) was the first to use a melt pond parameterization in the sea ice model, assuming a portion of the melted water could be retained at the ice surface. The retained water did not alter surface albedo and did not store any latent heat. The retained water refreezed during autumn so that the pond would have strong influence on sea ice thickness. Ebert and Curry (1993) also used a melt pond parameterization in their sea ice model, but they firstly considered the alteration of albedo at the sea ice surface. Taylor and Feltham (2004) developed a small-scale sea ice model, which simulated the physical processes that govern the evolution of melt pond depth and sea ice thickness. Lüthje et al. (2006) investigated the horizontal evolution of melt

Foundation item: The National Natural Science Foundation of China under contract No. 41406208; the Global Change Research of National Important Research Project on Science under contract No. 2015CB953900; the Scientific and Technology Development Fund of Shandong Academy under contract No. 2013QN042; the Key Program of National Natural Science Foundation of China under contract No. 41330960; the Open Research Fund of the State Oceanic Administration of the People's Republic of China Key Laboratory for Polar Science under contract No. 3KP201203.

*Corresponding author, E-mail: zhangshugang6@163.com

ponds over a summer melting season. Skyllingstad et al. (2009) used a melt pond model to predict pond size and depth change; the shortwave radiation absorbed in melt pond was parameterized in their model. Flocco et al.(2010, 2012, 2015) developed a simpler pond model which treats the refrozen ice growth as a classic Stefan phase change problem. And this model was incorporated into a climate sea ice model. Bogorodskiy and Marchenko (2014) developed a model which considers the refreezing of surface of melt pond in autumn, assuming that the temperature in whole melt pond could remain uniform because of sufficient convective mixing. These previous modeling studies have focused on the formation and evolution of melt pond. However the heat budget and the solar radiation allocation were little discussed in these models.

Here, we construct a one-dimensional thermodynamic model of melt pond on sea ice to study the thermodynamic processes of melt pond and melting process of pond covering ice in the High Arctic during the Chinese National Arctic Research Expedition carried out in the summer of 2010 (CHINARE-2010). In this model, solar radiation is the unique energy source for melt pond during CHINARE-2010. The objectives of this study were (1) to evaluate this model using measured data during CHINARE-2010, such as temperature, depth and net longwave radiation of melt pond and so on, (2) to calculate the heat budget of melt pond and the solar radiation allocation, and (3) to characterize the melt pond depth evolution on ice station.

2 Data observation and analysis

An ice station was established in the central Arctic located at 86.5°N and 172.4°W from August 12 to August 18, 2010 for an observational experiment of air-ice-ocean interactions. The ice thickness was 1.9 m on August 12. Solar radiation, longwave radiation, pond depth, pond temperature, and salinity were continuously measured at a typical melt pond (15.4 m×13.2 m) to study the thermodynamic processes of melt pond. Additionally, air temperature, surface pressure, air humidity, and velocity gradient were observed by a meteorological tower, which was installed on the sea ice.

Upward and downward radiations (including shortwave and longwave) were measured with a radiometer (CNR4, Kipp-Zonen), which was installed at a height of 0.6 m from melt pond surface. Because the field of view for lower detector is 150°, the CNR4 needs larger than 2.2 m far away from melt pond edge. In observation, the distance from melt pond edge to CNR4 is larger than 3 m. Data logger (CR1000, Campbell) recorded data every 10 min. The shortwave probe's measuring range is 0.3–2.8 μm and longwave probe's is 4.5–42 μm. The meteorological tower was composed of the Vaisala temperature and humidity probes (HMP45D), wind speed and direction sensors (05106 monitor-Ma, Young), and pressure sensors (CS106, Campbell), which were mounted at each height of 2, 4, and 10 m. A shortwave radiometer (CMA6, Kipp-Zonen) was mounted at the height of 1 m to calibrate CNR4, because it was more difficult to maintain CNR4 in a horizontal position at a melt pond than at the sea ice surface. Air-ice-ocean interaction data were obtained in the central Arctic from August 12 to 18, 2010.

Figure 1 shows the time series of 1-hour-mean downward solar radiation, denoted by irradiance, on the sea ice and melt pond. This figure indicates that the observed results between sea ice and melt pond are consistent, with a correlation coefficient of 0.98; the mean difference and the standard deviation (σ) are relatively small, being 6.9 and 8.4 W/m^2, respectively. Therefore, the observed data using CNR4 are accurate and can be used in the melt pond thermodynamic model.

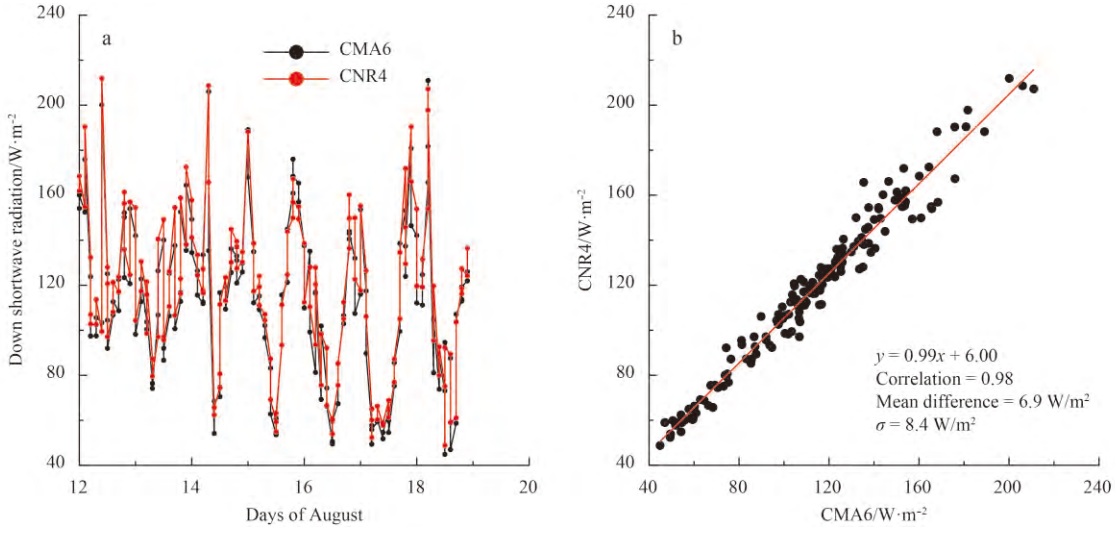

Fig. 1. Time series of 1-hour-mean downward solar radiation, denoted by irradiance, on the sea ice (red line) and melt pond (black line) from August 12 to 18, 2010 (a) and their correlation (b).

At the ice station, temperature, salinity and depth of 18 melt ponds (P01–P16) were measured from August 12 to 18 (Table 1). The results indicate that the temperature of the melt pond remained between 0.0°C and 0.2°C and the salinity remained between 0.1 and 0.4. Thus, both temperature and salinity changed very little during the observation period; in particular, salinity exhibited almost no change. The depths of melt ponds were between 38 cm and 53 cm on August 12, and between 45 cm and 56 cm on August 18. There were three melt ponds whose depths did not change, while the others changed by 5–10 cm.

Figure 2 shows the profiles of temperature and salinity at P08, P09 and P13a on August 12 and 18. All of these profiles indicate that the temperature and salinity were all uniform at the whole vertical range. The salinity of melt ponds is caused by sea ice brine when sea ice melts. Driven by solar radiation, turbulent convective motion existed across the entire pond, and main-

Table 1. Temperature (T), salinity (S) and depth (D) of melt pond

Name	August 12			August 18			Change		
	T/°C	S	D/cm	T/°C	S	D/cm	T/°C	S	D/cm
P01	0.09	0.11	45	0.14	0.10	45	0.05	–0.01	0
P02	0.09	0.09	38	0.09	0.08	45	0.00	–0.01	7
P03	0.12	0.10	39	0.06	0.08	49	–0.06	–0.02	10
P04	0.09	0.08	47	0.12	0.10	52	0.03	0.02	5
P05a	0.09	0.10	39	0.06	0.11	46	–0.03	0.01	7
P05b	0.14	0.11	40	0.09	0.11	47	–0.05	0.00	7
P06	0.12	0.12	46	0.06	0.11	52	–0.06	–0.01	6
P07	0.18	0.28	45	0.15	0.25	48	–0.03	–0.03	3
P08	0.15	0.12	49	0.07	0.12	53	–0.08	0.00	4
P09	0.17	0.12	50	0.05	0.12	56	–0.12	0.00	6
P10	0.12	0.09	44	0.07	0.09	50	–0.05	0.00	6
P11	0.17	0.11	45	0.08	0.11	51	–0.09	0.00	6
P12	0.16	0.12	50	0.07	0.12	55	–0.09	0.00	5
P13a	0.16	0.15	51	0.06	0.16	56	–0.10	0.01	5
P13b	0.12	0.15	50	0.04	0.16	54	–0.08	0.01	4
P14	0.18	0.42	48	0.34	0.39	48	0.15	–0.08	0
P15	0.26	0.43	53	0.17	0.37	55	–0.09	–0.06	2
P16	–0.02	0.39	51	0.35	0.39	51	0.37	0.00	0

Note: All data are observed from 8 clock to 9 clock (UT) for each day.

tained a uniform temperature and salinity in the whole melt pond column (Taylor, 2004).

3 Model description

3.1 *Heat transport within melt pond*

3.1.1 *Radiative transfer process of melt pond*

First, melt pond formation is driven by the summertime increase of solar radiation. Second, there have different absorptions of solar radiation with different bands in water. Third, the solar radiation data measured using CNR4 and CMA6 denote total energy of solar radiation. So here we need to adopt a more sophisticated radiation model.

Solar radiation parameterization is used during the Surface Heat Budget of the Arctic Ocean (SHEBA) experiment (Pegau, 2002). It can be written as

$$F_{\mathrm{r}}(z)\downarrow = P_n(1-R_0)I_0F_{\mathrm{SW}}(1-\mathrm{e}^{-K_nz}), \tag{1}$$

where P_n is the fraction of radiation in band n, I_0 is the fraction of radiation that is not absorbed near the melt pond surface and is set to 0.6 (Taylor and Feltham, 2004), R_0 is the Fresnel reflection coefficient and is equal to 0.05 (Perovich, 1990), F_{SW} is the incident irradiance, K_n is the diffuse extinction coefficient in band n, and z is the depth below the melt pond surface. Parameters in different bands are presented in Table 2. When solar radiation reaches the pond-covered ice surface, some radiation is reflected at the ice surface, while others are transmitted into the ice. The albedo of pond-covered ice is related to ice types, it ranges from 0.2 to 0.7 (Podgorny and Grenfell, 1996). Parameterization of reflected radiation in melt pond can be written as

$$F_{\mathrm{r}}(z)\uparrow = P_n\alpha_{\mathrm{b}}F_{\mathrm{r}}(z_{\mathrm{b}})(1-\mathrm{e}^{-K_n[(z_{\mathrm{b}}-z)+z_{\mathrm{b}}]}), \tag{2}$$

where $F_{\mathrm{r}}(z_{\mathrm{b}})$ is the solar radiation at the bottom of pond, z_{b} is the depth of pond, and α_{b} is the albedo of pond-covered ice. Heating of the melt pond is calculated as a function of pond depth by integrating Eqs (1) and (2):

$$Q_{\mathrm{r}} = \int_h F_{\mathrm{r}}(z)\downarrow \mathrm{d}z + \int_h F_{\mathrm{r}}(z)\uparrow \mathrm{d}z. \tag{3}$$

Equations (1) and (2) can be used not only to calculate the albedo of pond but also to obtain the radiation ($F_i(z_{\mathrm{b}})$) that is transmitted into the ice:

$$F_{\mathrm{i}}(z_{\mathrm{b}}) = (1-\alpha_{\mathrm{b}})F_{\mathrm{r}}(z_{\mathrm{b}}). \tag{4}$$

Radiation absorbed in the sea ice is calculated using the Beer's Law:

$$F_{\mathrm{i}}(z) = F_{\mathrm{i}}(z_{\mathrm{b}})\,\mathrm{e}^{-\beta(z-z_{\mathrm{b}})}, \tag{5}$$

where β is the bulk extinction coefficient in the ice, which is set to 1.5 m^{-1} (Untersteiner, 1961).

3.1.2 *Thermodynamic process of melt pond*

Melt ponds contain certain salinity due to small volume of brine in the sea ice. Therefore, the freezing temperature T_f of melt pond is derived from a simplified relationship:

$$T_f = -mS, \tag{6}$$

where m=0.055 (Yu and Rothrock, 1996), S is salinity of melt pond. The melt pond becomes dynamically unstable under the action of solar radiation, which could be judged using the Rayleigh number ($Ra(t)$):

$$Ra(t) = \frac{g\alpha^*\Delta TH_{\mathrm{p}}^3}{\upsilon\kappa}, \tag{7}$$

where α^*=5×10^{-5} K^{-1} is the coefficient of thermal expansion of

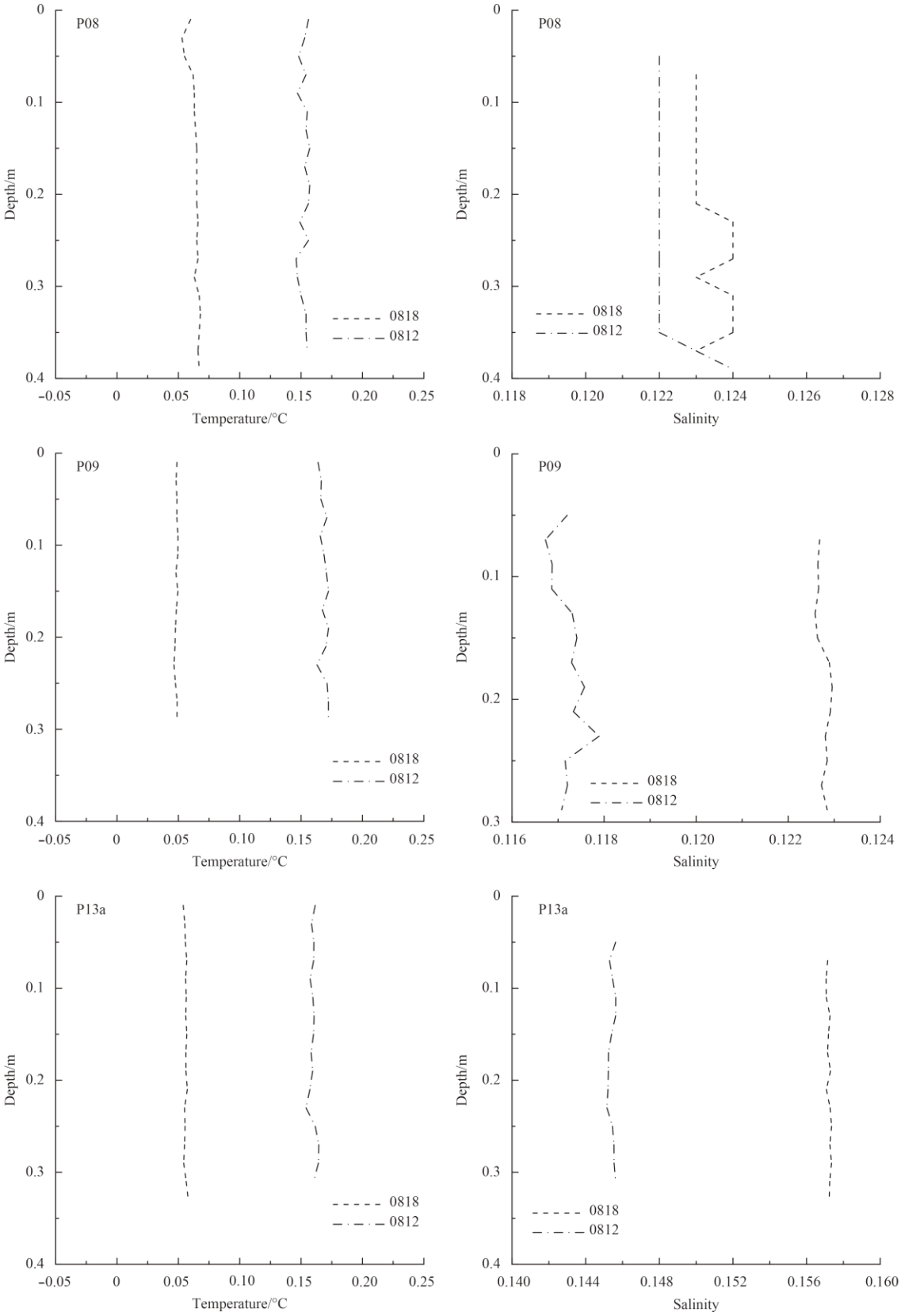

Fig. 2. Profiles of temperature and salinity at Sites P08, P09 and P13a.

melt pond water, g=9.81 m/s² is the acceleration due to gravity, κ=1.19×10⁻⁷ m²/s is the thermal diffusivity of melt pond, υ=10⁻⁶ m/s is the kinematic viscosity of the water in the melt pond, ΔT is the temperature difference across the pond, and H_p is the depth of melt pond. The critical Rayleigh number (Ra_{crit}) is 630. Taylor (2004) indicated that $Ra(t)$ will be much larger than Ra_{crit} for a 0.1

Table 2. Absorption parameters of fresh water at different bands of solar radiation

Wavelength range/nm	P_n	K_n
350–700 (n=1)	0.481	0.18
700–900 (n=2)	0.194	3.25
900–11 000 (n=3)	0.123	27.5
>1 100 (n=4)	0.202	300

m melt pond. Such large $Ra(t)$ leads to turbulent convective motion across the entire pond; thus, the temperature of the whole melt pond becomes relatively uniform. In this case, the core temperature ($\overline{T}$) of melt pond can be written as

$$(\rho c)_{\mathrm{p}} H_{\mathrm{p}} \frac{\partial \overline{T}}{\partial t} = -F_{\mathrm{c}}(T_{\mathrm{l}}) - F_{\mathrm{c}}(T_{\mathrm{u}}) - \int_{h_u}^{h_l} \frac{\partial}{\partial z} F_{\mathrm{net}}(z)\mathrm{d}z, \tag{8}$$

where T_{l} and T_{u} are the temperature at the lower and upper boundaries of the pond, respectively, $(\rho c)_{\mathrm{p}}$=4.185×10^6 J/(m^3·K) is the volumetric specific heat capacity of the pond, $\int_{h_u}^{h_l} \frac{\partial}{\partial z} F_{\mathrm{net}}(z)\mathrm{d}z$ is the absorbed solar radiation of melt pond, and $F_{\mathrm{c}}(T_{\mathrm{l}})$ and $F_{\mathrm{c}}(T_{\mathrm{u}})$ are the heat fluxes of lower and upper boundary layers, respectively. In the boundary layer, heat flux is assumed to be independent of the depth of the boundary layer; so the heat flux out of the liquid layer at the upper boundary is given by (Taylor and Feltham, 2004):

$$F_{\mathrm{c}}(T^*) = \mathrm{sgn}(\overline{T} - T^*)(\rho c) J \left|\overline{T} - T^*\right|^{4/3} \quad Ra(t) \geqslant Ra_{\mathrm{crit}}, \tag{9}$$

where T^* is the boundary temperature (namely, T_{u} or T_{l}), and

$$J = \gamma\left(\frac{g\alpha^* \kappa^2}{\upsilon}\right)^{1/3}, \tag{10}$$

where γ=0.1 is a constant.

3.2 *Heat transport within sea ice*

Heat transfer within the sea ice is given by

$$(\rho_{\mathrm{i}} c_{\mathrm{i}}) \frac{\partial T}{\partial t} = \frac{\partial}{\partial z}\left(\kappa_{\mathrm{i}} \frac{\partial T}{\partial z}\right) + \frac{\partial}{\partial z} F_{\mathrm{i}}(z), \tag{11}$$

where T is sea ice temperature, c_{i} is the specific heat capacity of sea ice, ρ_{i} is sea ice density, and $F_{\mathrm{i}}(z)$ is the solar radiation that passes through the melt pond and enters the sea ice. Note that the standard density of sea ice is 917 kg/m^3. Untersteiner (1961) experimentally derived c_{i} as a function of sea ice temperature and salinity:

$$c_{\mathrm{i}}(T, S) = c_0 + \frac{\gamma S}{(T - 273)^2}, \tag{12}$$

where c_0=2 110 J/(kg·K) is the heat capacity of fresh ice, $\gamma = L_0\mu$, where μ is equal to 0.054, and L_0=334 kJ/kg is the latent heat of fusion of fresh ice. κ_{i} is the thermal conductivity of ice, which is also a function of sea ice temperature and salinity (Bitz and Lipscomb, 1999):

$$\kappa_{\mathrm{i}}(T, S) = \kappa_0 + \frac{\lambda S}{T - 273}, \tag{13}$$

where κ_0=2.034 W/(m·K) is the conductivity of fresh ice, and λ=0.117 W/m. The salinity of sea ice is 4.

3.3 *Boundary conditions*

3.3.1 *Melt pond/atmosphere boundary*

The net heat flux at the interface between melt pond and atmosphere is given by

$$E_{\mathrm{pond}} = F_{\mathrm{c}}(T_0) + F_{\mathrm{LW}} - \varepsilon\sigma T_0^4 + (1 - i_0)\times (1 - \alpha)F_{\mathrm{SW}} + F_{\mathrm{sens}} + F_{\mathrm{lat}}, \tag{14}$$

where F_{SW} and F_{LW} are the incoming shortwave and longwave radiations, respectively, which can be measured. $F_{\mathrm{c}}(T_0)$ is the heat flux at the surface of the pond, i_0=0.6 (Taylor and Feltham, 2004) is the fraction of incoming radiation that penetrates into the melt pond, α is the albedo of melt pond surface, ε is the emissivity of the pond, σ=5.67×10^{-8} is the Stefan-Boltzmann constant, T_0 is the temperature at the surface of the pond, and F_{sens} and F_{lat} are sensible and latent heat fluxes at the melt pond surface, respectively. F_{sens} and F_{lat} are defined respectively by

$$F_{\mathrm{sens}} = \rho_{\mathrm{a}} c_{\mathrm{p}} C_{\mathrm{s}} u(T_{\mathrm{a}} - T_0), \tag{15}$$

$$F_{\mathrm{lat}} = \rho_{\mathrm{a}} L_{\mathrm{v}} C_{\mathrm{l}} u(q_{\mathrm{a}} - q_0), \tag{16}$$

where ρ_{a}=1.275 kg/m^3 is the density of dry air, c_{p}=1 005.0 J/(kg·K) is the specific heat capacity of dry air, L_{v}=2.49 MJ/kg is the latent heat of vaporization, C_{s} and C_{l} are the turbulent exchange coefficients of sensible heat and latent heat, respectively, T_{a} is air temperature, u is wind speed, q_{a} is the specific humidity of air, and q_0 is the specific humidity at the surface. q_0 is calculated by

$$q_0 = \frac{0.622 p_v}{p_{\mathrm{atm}} - 0.378 p_v}, \tag{17}$$

where p_{atm} is atmospheric pressure at the ice surface, p_v=2.53×10^8 exp(–5 420/T_0), and its units are kPa (Rogers and Yau, 1989). Here C_{s} and C_{l} are related to atmospheric stability. Bian et al. (2011) calculated C_{s} and C_{l} using the meteorological data observed during the 2008 Chinese National Arctic Research Expedition. The result suggested that turbulent exchange coefficient (C_{s} or C_{l}) should be equal to 1.6×10^{-3} at neutral stratification. Louis (1979) gave the expression of turbulent exchange coefficient at stable stratification and unstable stratification, respectively:

$$C = C_0\left(1 - \frac{2b'Ri}{1 + c|Ri|^{1/2}}\right) \quad Ri < 0, \tag{18a}$$

$$C = C_0(1 + b'Ri)^{-2} \quad Ri \geqslant 0. \tag{18b}$$

In the above equations, Ri is the bulk Richardson number,

$$Ri = \frac{g(T_{\mathrm{a}} - T_0)\Delta z}{T_{\mathrm{a}} u}, \tag{19}$$

where Δz is 10 m, c=1.6×10^{-4} m is ice surface parameter, b' =20 (Ebert and Curry, 1993), and C_0 is turbulent exchange coefficient for the neutral stratification. In the calculation of turbulent heat flux, C equals to C_{s} (or C_{l}). When T_0 is lower than the freezing

temperature (T_f), the melt pond would refreeze at surface. The actual observations suggest that the refresh ice should float at the melt pond surface; however, it is too thin to be measured. So T_f is used in Eq. (8) when the melt pond surface has refreshing ice.

3.3.2 *Melt pond/sea ice boundary*

In the models of Taylor and Feltham (2004), Lüthje et al. (2006), and Skyllingstad et al. (2009), the melting rate of the upper pond-covered ice equals to the rate of change of melt pond depth. However, there are large differences compared to actual observations. The temperature of pond-covered ice would rise due to the effects of solar radiation and heat conduction of pond water. The pond-covered ice melts once it is heated to a temperature higher than its melting point. The more heat the ice absorbs, the more obviously the ice melts. The layer of ice will melt completely when the absorbed energy is larger than the latent heat required by melting.

When the temperature of pond-covered ice is higher than its melting point, the absorbed energy can be calculated by

$$\rho_i c_i (T_i - T_f) = \kappa_i \frac{\partial^2 T_i}{\partial z^2} \mathrm{d}t_1 + \beta F_i(z_b) \exp(-\beta(z - z_b)) \mathrm{d}t_1 \quad (20a)$$

or

$$Q_\Delta = \rho_i c_i \frac{\Delta T}{\mathrm{d}t_1} = \kappa_i \frac{\partial^2 T_i}{\partial z^2} + \beta F_i(z_b) \exp(-\beta(z - z_b)), \quad (20b)$$

where $\mathrm{d}t$ is the time step, $\mathrm{d}t_1$ is the time that T_i reaches T_f. $\mathrm{d}t_2$ is one time step after $\mathrm{d}t_1$,

$$\mathrm{d}t_1 = \frac{\rho_i c_i (T_f - T_i)}{\kappa_i \frac{\partial^2 T}{\partial z^2} + \beta F_i(z_b) \exp(-\beta(z - z_b))}, \quad (21)$$

$$\mathrm{d}t_2 = \mathrm{d}t - \mathrm{d}t_1. \quad (22)$$

Thus, the accumulated energy during $\mathrm{d}t_2$ is derived by

$$Q_{top} = [F_c(T_l) + F_i(z_b) - F_i(z_b) \exp(-\beta \Delta z) - (\kappa \frac{\partial T}{\partial z})_{top}] \mathrm{d}t_2. \quad (23)$$

Equations (1) to (23) are used to analyze melt pond formation and pond-covered ice's heat balance. It should be noted: (1) The salinity of melt pond changes very little, and it is not affected by brine during pond-covered ice melting. (2) The albedo of pond-covered ice can be estimated by observed downward and upward solar radiations, while the absorbed radiation by melt pond and ice is calculated by parametric equations. (3) Ice melting process could not be calculated using the depth change of melt pond since sea ice is densely layered in the model (Δz=0.01 m), and the melting rate of pond-covered ice is the number of melting layers per unit of time.

3.4 *Method of solution*

The governing equations solved within each domain are decoupled. First, the boundary condition of melt pond/atmosphere provides the surface temperature of melt pond which is necessary for Eq. (8). Second, the governing equations of melt pond and radiative transfer equations provide the melt pond temperature. Third, governing equations of sea ice provide the sea ice temperature for each layer. At last, the heat flux and melt pond depth could be calculated by relevant equations.

During each time step, the input data (such as air temperature, humidity, wind speed, solar radiation and longwave radiation and so on) and the depth of melt pond are considered to be fixed. At the end of each time step the input data are updated. Once accumulated energy for each sea ice layer (0.01 m) becomes greater than the melting energy, the melt pond depth will increase 0.01 m. Then the boundary conditions will change in the next time step and the depth of melt pond will also be updated.

4 Evaluation and simulation

Some simulation results can be evaluated by measured data during CHINARE-2010 period, such as net long wave radiation, temperature and depth of melt pond. Then we can reasonably analyze the heat budget and depth evolution of melt pond.

4.1 *Evaluation*

The status of the melt pond surface changed continuously during the observation period. Overall, the melt pond surface was covered with fresh ice before August 17 and fresh ice was absent after August 17. Sandven and Johannesen (2006) noted that melt pond behaves almost as a black body at the infrared wavelengths, namely, the emissivity of melt pond is approximately equal to 1.00. However, the emissivity of sea ice is approximately 0.97 (Ebert and Curry, 1993). Therefore, the emissivity of melt pond is constant when it has no fresh ice or is entirely covered with fresh ice. When the melt pond surface is partially covered, its emissivity is between 0.97 and 1.00. The emissivity of melt pond surface decreased linearly from 1.00 to 0.97 before August 16, and increased linearly from 0.97 to 1.00 on August 16 (from 00:00 to 23:00); thereafter, its value was equal to 1.00.

Figure 3a shows that the simulated and measured net longwave radiations are similar except around August 15. The actual survey found that the melt pond surface changed rapidly around August 15. This means the radiation condition of melt pond was obviously changed by the transformation of the melt pond surface. Figure 3b reveals that the correlation coefficient reaches 0.96, and that the mean difference and the standard deviation are relatively small (1.5 and 1.9 W/m^2, respectively) between measured and simulated results. Therefore, the model can be used for analyzing the thermodynamic processes of the melt pond.

The melt pond surface sometimes had a new ice crust with the thickness no more than 1 cm, which had an inevitable effect on the radiative fluxes of the melt pond surface. The radiation absorbed by the new ice crust was calculated using Eq. (5). The bulk extinction coefficient in new ice is thought to be 0.60–0.78 m^{-1} (Bolsenga, 1978; Heron and Woo, 1994). If the bulk extinction coefficient and thickness of the new ice crust were assumed to be 0.78 m^{-1} and 0.01 m, respectively, the new ice crust would absorb only 0.8% of the incoming solar radiation. However, the fraction of solar radiation absorbed by the ice crust would be less than the amount predicted using the model, meaning that almost all incoming solar radiation would enter the melt pond.

Figure 4 shows comparison of the simulated temperatures to the measured ones using ALEC-CTD data on August 12 and 18. The figure illustrates that the melt pond temperature exhibited a diurnal cycle, which is due to the diurnal variation of solar radiation. It also indicates that the differences between simulated and measured temperatures are 0.02°C and 0.03°C on August 12 and 18, respectively. Therefore, the model simulated the temperature of melt pond fairly well.

4.2 *Heat budget of melt pond*

Solar radiation is the energy source for melt pond in summer-

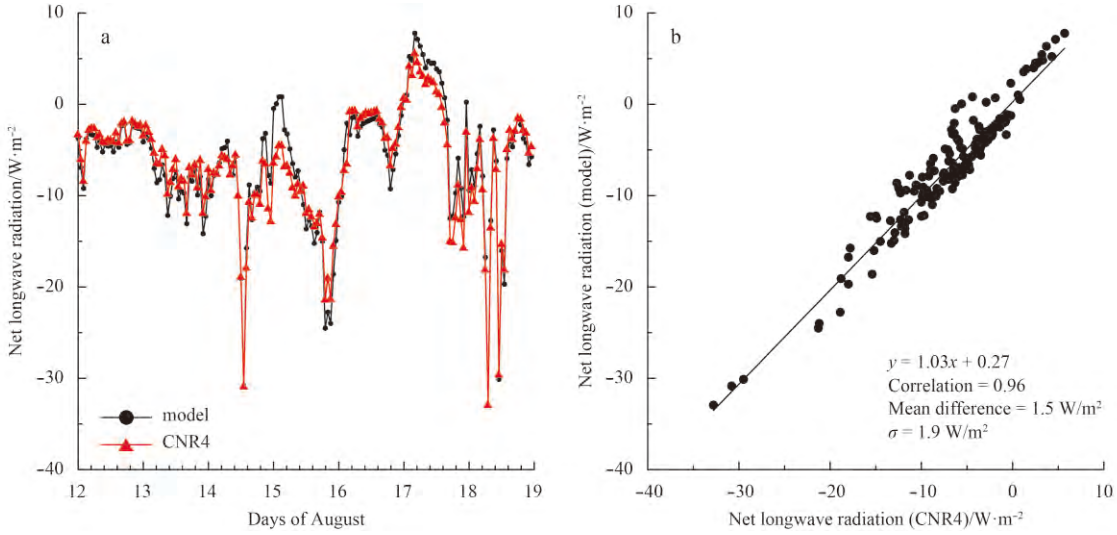

Fig. 3. Time series of simulated and measured net longwave radiation at the melt pond surface using the model and CNR4, respectively (a), and the correlation between simulated and measured results (b).

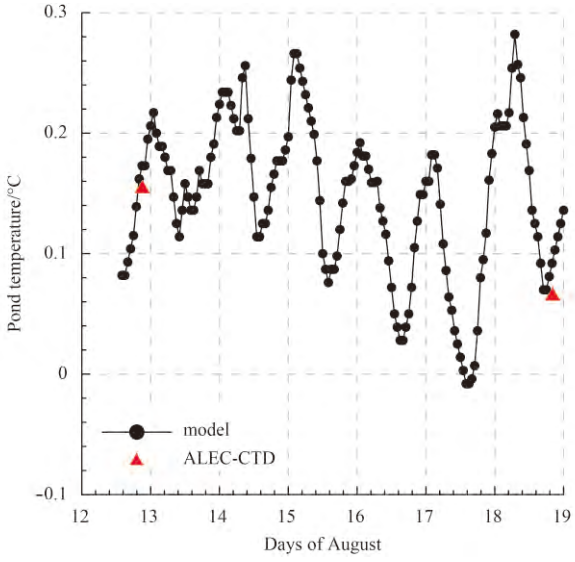

Fig. 4. Times series of simulated temperature (black line) of melt pond using the model and measured data (red triangles) using ALEC-CTD during August 12–18.

time in the central Arctic. Thus, it is important to quantitatively examine the heat budget of the melt pond surface and its transformation, such as net longwave radiation, sensible heat, latent heat, melt pond temperature and pond-covered ice melting and so on.

Figure 5 shows the times series of simulated sensible and latent heat fluxes during the observation period. At melt pond/atmosphere interface, melt pond release partial energy of solar radiation in the form of net longwave radiation (Fig. 3a), sensible heat (Fig. 5a) and latent heat (Fig. 5b). Sensible heat flux was negative before August 17, with a minimum of –40 W/m^2. However, it became positive on August 18, with a maximum of 20 W/m^2. Latent heat flux was negative from August 12 to 18, with a minimum of –25 W/m^2 on August 18. The results suggest that melt pond transported heat to the atmosphere in the forms of sensible heat and latent heat most of the time.

Section 3.1 of this paper shows that when solar radiation enter melt pond, partial solar radiation are absorbed by melt pond water and pond-covered ice, respectively (Figs 6a and b). From Fig. 6, we know that the heat flux absorbed by melt pond and pond-covered ice have a diurnal period. And melt pond absorbed is larger than pond-covered ice.

The total incident and reflected radiations of melt pond were 60.7 and 8.8 MJ/m^2 during the observation period; this means the average reflectance of melt pond was 0.15, and 85% of the total solar radiation energy entered the melt pond. Table 3 presents the total amount of radiation and heat balance flux at surface and inside of the melt pond from August 12 to 18. It indicates that 12.3% and 7.5% of the net solar radiation were lost in the form of sensible heat and latent heat, respectively. The turbulent exchange coefficient is an important parameter; the choice of its value can cause inaccuracy in calculations of sensible heat and latent heat, though this inaccuracy is generally very small (Ebert and Curry, 1993; Taylor and Feltham, 2004). Therefore, we can see that a large amount of net solar radiation was absorbed by the melt pond, which was used to warm melt pond and melt pond-covered ice (including bottom ice and lateral ice of melt pond). The simulated results suggest that 58.6% of the solar radiation should enter into the pond-covered ice. The allocation of entering melt pond solar radiation are summarized in Fig. 7.

4.3 *Melt pond depth evolution*

Diurnal variation of melt pond temperature shows that although the melt pond absorbed a large amount of solar radiation, its temperature did not increase with time. Thus, absorbed energy must be transformed into other forms of energy in order to maintain the same temperature for melt pond water. The melt pond depth at P08 changed only 4 cm between August 12 and 18 (Table 1). Calculation suggests that only 13 MJ/m^2 of heat would be needed to melt the pond-covered ice of 4 cm. This amount is much smaller than the energy of 30.4 MJ/m^2 absorbed by pond-covered ice, as shown in Table 3. The depth of a melt pond will vary not only with the melting of pond-covered ice, but also in response to many other factors, such as melting of the sea ice surface and penetration of melt pond water into sea ice (Cox and Weeks, 1974; Weeks and Ackley, 1986; Notz, 2005). The energy

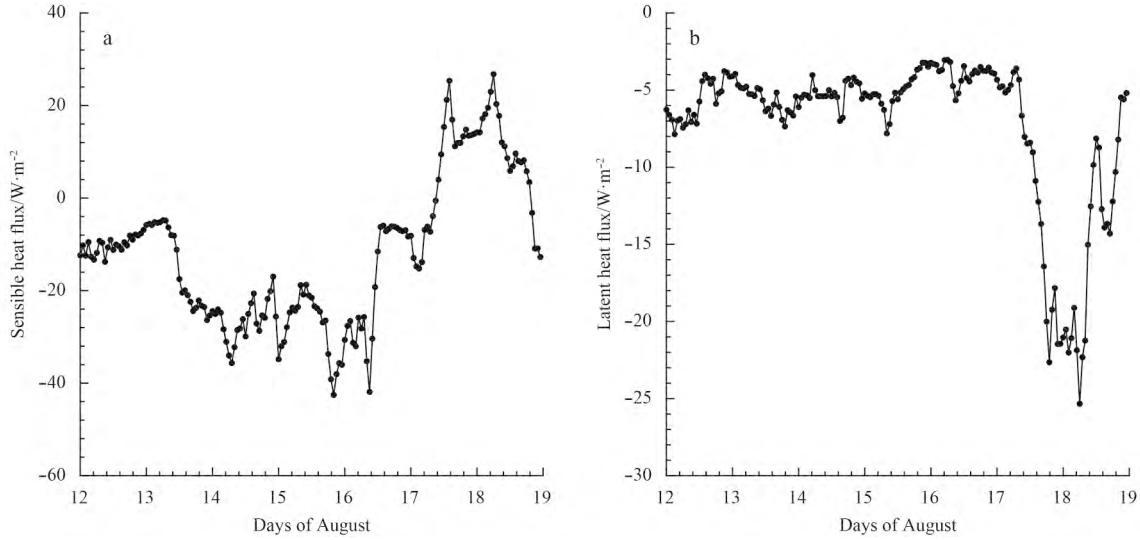

Fig. 5. Time series of simulated sensible heat flux (a) and latent heat flux (b) obtained using the model.

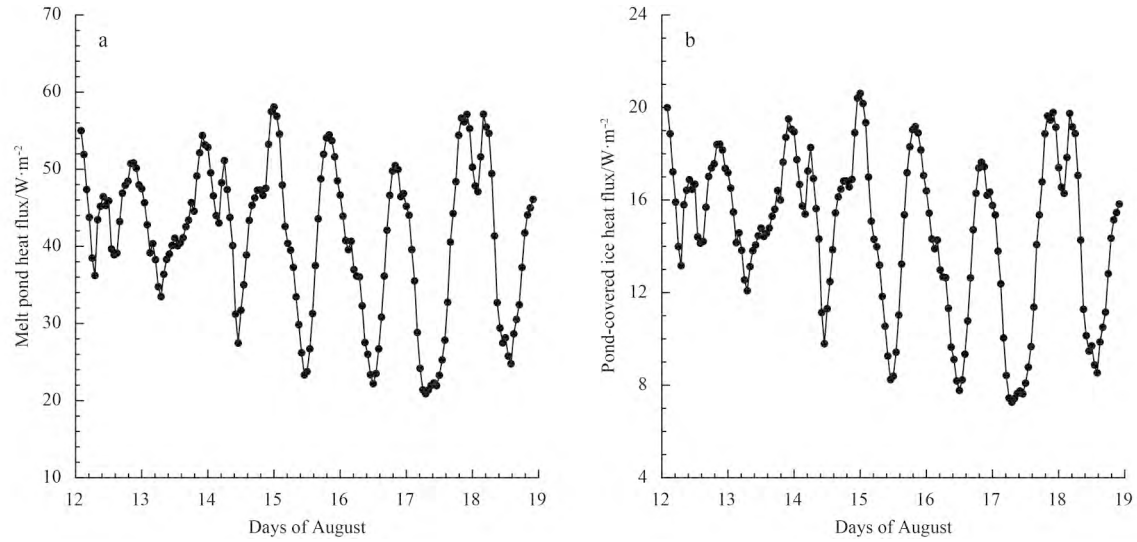

Fig. 6. Times series of simulated melt pond heat flux (a) and pond-covered ice heat flux (b).

Table 3. The total energy of radiation and heat flux at the surface and inside of the melt pond during August 12–18

Name	NS	NL	SH	LH	IP	MP	RS
Total energy/MJ·m^{-2}	51.9	–3.6	–6.4	–3.9	–7.4	–0.2	–30.4

Note: NS represents net solar radiation, NL net longwave radiation, LH latent heat, SH sensible heat, IP radiation entering into pond-covered ice, MP melt pond obtained radiation, and RS remainder.

accumulation model was used to study the melting rate of pond-covered ice. Figure 8 shows the times series of simulated pond-covered ice melting. Pond-covered ice lost nearly 8 cm at its upper surface from August 12 to 18 (about 1 cm/d). The simulated results suggest that about 25 MJ/m^2 of the 30.4 MJ/m^2 (Table 3) was used to melt the sea ice with 8 cm thick and the remainder (about 5.4 MJ/m^2) was used to warm the pond-covered ice.

For this sea ice station, Lei et al. (2012) indicated that the sea ice bottom had decayed by 5.3 cm during August 9–18, with a mean melt rate of (0.5±0.2) cm/d. So we know that the melt rate of upper pond-covered ice is larger than the snow-covered ice (around two times). Xie et al. (2013) indicated that the lower melt rate of pond-covered ice also larger than that of the snow-covered ice. So we know also that the sea ice within melt pond have faster melt rate than that of sea ice without melt pond. So this coincide with the result of Fetterer and Untersteiner (1998) that the melting speed of pond-covered ice is estimated to be between 2 and 3 times faster than that of bare ice.

The above analysis suggests that the solar radiation was mainly used to melt sea ice. Equations (1) and (2) indicate that the amount of solar radiation absorbed by a melt pond with greater depth is also greater. Therefore, melt ponds with different depths can exhibit different changes in melting, even under the same weather conditions and with the same incoming solar radiation. Figure 9 shows the average amount of pond-covered ice melting at different initial depths of melt pond from August 12

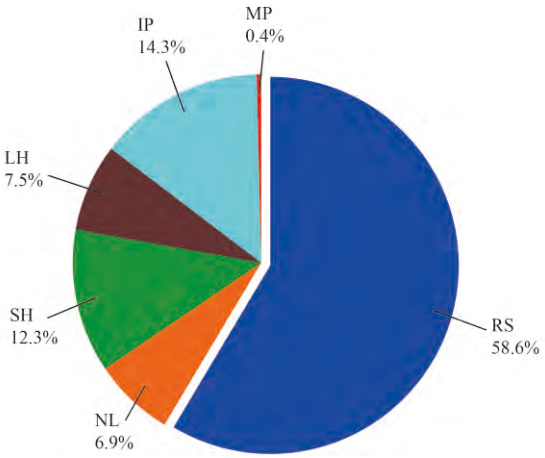

Fig. 7. Allocation of entering melt pond sola radiation.

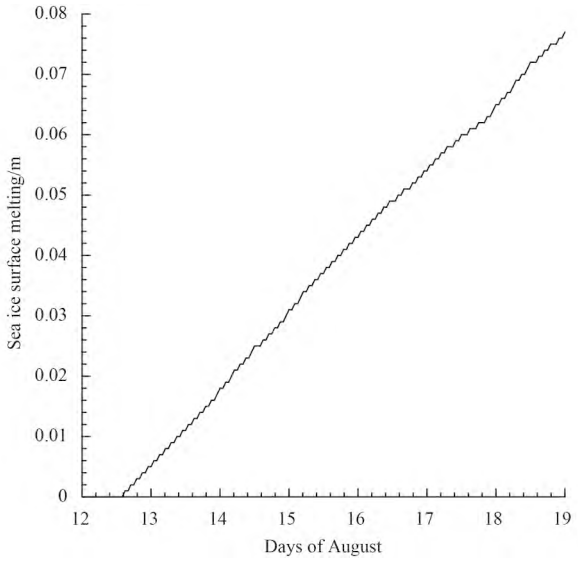

Fig. 8. Times series of simulated pond-covered ice melting.

to 18. The melting rate of pond-covered ice changed rapidly with the initial depth of less than 0.4 m; however, the melting rate did not change much (about 1 cm/d) for melt ponds deeper than 0.4 m. Almost all of the melt ponds at the ice station had depths exceeding 0.4 m; therefore, melting rate was relatively constant.

5 Conclusions

In this paper, a one-dimensional thermodynamic model of melt ponds is established and some measured data, such as net longwave radiation, water temperature and depth of melt pond, are used to test this model. Then thermodynamic processes of melt pond and pond-covered ice melting are simulated by using observing data of CHINARE-2010. The results indicate that melt ponds not only play important role in the rapid change of Arctic sea ice but also provide important evidence to study the climate change of Arctic. The main results are as follows:

(1) The temperature of melt pond is reasonably simulated under two conditions that refreezing exists at the surface of melt pond and the depth of the melt pond is treated as an external parameter. The simulated temperature of melt pond had a diurnal variation and its value ranged between 0.0°C and 0.3°C.

(2) About 85% of the incident solar radiation passes through

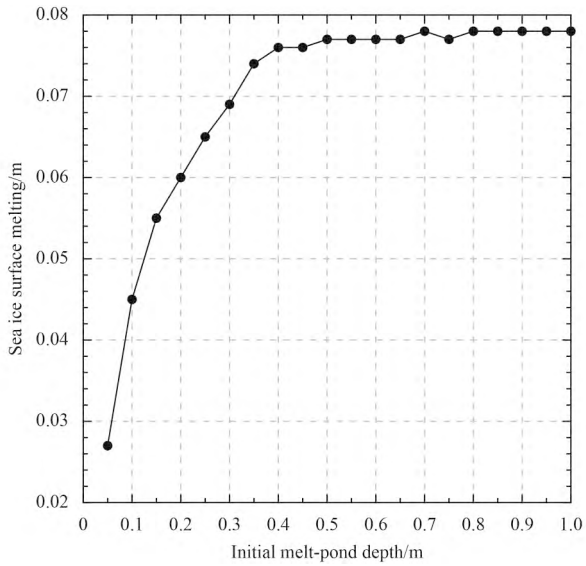

Fig. 9. The average amount of pond-covered ice melting at different initial depths from August 12 to 18.

the melt pond surface, and some of it was released in the form of sensible and latent heat. However, the released energy was very little (about 15%), compared to the incident solar radiation. More than 58.6% of the incident energy was absorbed by melt pond water, which caused pond-covered ice melting and diurnal variation of pond water temperature.

(3) The melting rate of upper pond-covered ice is estimated to be around 2 times faster than snow-covered ice. At the same time, the change of melting rate was relatively quick for pond depth less than 0.4 m, while the melting rate remained relatively constant (about 1.0 cm/d) for pond with depth greater than 0.4 m.

Based on some parametric equations, especially with the parameterization of solar radiation, we have established a model which could provide a realistic simulation of the heat flux and depth of melt pond. But this model is just in an initial stage in our study, because some special cases, such as the melt pond with fresh water, may need to be considered. When pond-covered ice melts, massive amount fresh water may suddenly enter into upper layer of ocean, and cause strong halocline in a certain time. So it is very important to know the evolution of fresh water mass transport due to melting of sea ice. Second, when pond-covered ice melts, more solar radiation would enter into the upper ocean. This will unavoidably change the heat flux between sea and atmosphere. Furthermore, some distinctive phenomenon would appear, for example, near surface temperature maximum and thermocline at upper ocean will change. As Arctic climate and sea ice conditions continue to change, the melt pond will play more and more important role in sea ice melting, heat flux, fresh water flux and climate models. So it is worth to continue study on the melt pond in future.

Acknowledgements

The authors gratefully acknowledge the expedition members of CHINARE-2010 and R/V *Xuelong* crew for their help.

References

Bian Lingen, Ma Yongfeng, Lu Changgui. 2011. Experiment of turbulent flux near surface layer and its parameterizations on a drift ice over the Arctic Ocean. Haiyang Xuebao (in Chinese), 33(2): 27–35

Bitz C M, Lipscomb W H. 1999. An energy-conserving thermodynamic model of sea ice. J Geophys Res, 104(C7): 15669–15677

Bogorodskiy P V, Marchenko A V. 2014. Thermodynamic effects accompanying freezing of two water layers separated by a sea ice sheet. Oceanology, 54(2): 152–159

Bolsenga S J. 1978. Photosynthetically active radiation transmittance through ice. NOAA Technical Memorandum ERL GLERL-18. Ann Arbor, Michigan: Great Lakes Environmental Research Laboratory, US Department of Commerce

Cox G F N, Weeks W F. 1974. Salinity variations in sea ice. J Glaciol, 13(67): 109–120

Ebert E E, Curry J A. 1993. An intermediate one-dimensional thermodynamic sea ice model for investigating ice-atmosphere interactions. J Geophys Res, 98(C6): 10085–10109

Eicken H, Gradinger R, Ivanov B, et al. 1996. Surface melt puddles on multi-year sea ice in the Eurasian Arctic. In: Proceedings of ACSYS Conference on the Dynamics of the Arctic Climate System World Climate Research Programme. Göteborg, Sweden: WMO/TD, 267–271

Fetterer F, Untersteiner N. 1998. Observations of melt ponds on Arctic sea ice. J Geophys Res, 103(C11): 24821–24835

Flocco D, Feltham D L, Turner A K. 2010. Incorporation of a physically based melt pond scheme into the sea ice component of a climate model. J Geophys Res, 115(C8): C08012, doi: 10.1029/2009JC005568

Flocco D, Schroeder D, Feltham D L, et al. 2012. Impact of melt ponds on Arctic sea ice simulations from 1990 to 2007. J Geophys Res, 117(C9): C09032, doi: 10.1029/2012JC008195

Flocco D, Feltham D L, Bailey E, et al. 2015. The refreezing of melt ponds on Arctic sea ice. J Geophys Res, 120(2): 647–659, doi: 10.1002/2014JC010140

Grenfell T C, Maykut G A. 1977. The optical properties of ice and snow in the Arctic Basin. J Glaciol, 18(80): 445–463

Heron R, Woo M K. 1994. Decay of a high Arctic lake-ice cover: observations and modelling. J Glaciol, 40(135): 283–292

Landy J, Ehn J, Shields M, et al. 2014. Surface and melt pond evolution on landfast first-year sea ice in the Canadian Arctic Archipelago. J Geophys Res, 119(5): 3054–3075

Lei Ruibo, Zhang Zhanhai, Matero I, et al. 2012. Reflection and transmission of irradiance by snow and sea ice in the central Arctic Ocean in summer 2010. Polar Res, 31(1): 17325, doi: 10.3402/polar.v31i0.17325

Louis J F. 1979. A parametric model of vertical eddy fluxes in the atmosphere. Boundary-Layer Meteor, 17(2): 187–202

Lüthje M, Feltham D L, Taylor P D, et al. 2006. Modeling the summertime evolution of sea-ice melt ponds. J Geophys Res, 111(C2): C02001, doi: 10.1029/2004JC002818

Maykut G A, Untersteiner N. 1971. Some results from a time-dependent thermodynamic model of sea ice. J Geophys Res, 76: 1550–1575

Mellor G L, Kantha L. 1989. An ice-ocean coupled model. J Geophys Res, 94(C8): 10937–10954

Notz D. 2005. Thermodynamic and fluid-dynamical processes in sea ice [dissertation]. Cambridge: University of Cambridge

Pegau W S. 2002. Inherent optical properties of the central Arctic surface waters. J Geophys Res, 107(C10): 8035, doi: 10.1029/2000JC000382

Perovich D K. 1990. Theoretical estimates of light reflection and transmission by spatially complex and temporally varying sea ice covers. J Geophys Res, 95(C6): 9557–9567

Perovich D K, Grenfell T C, Light B, et al. 2002. Seasonal evolution of the albedo of multiyear Arctic sea ice. J Geophys Res, 107(C10): 8044, doi: 10.1029/2000JC00438

Podgorny I A, Grenfell T C. 1996. Partitioning of solar energy in melt ponds from measurements of pond albedo and depth. J Geophys Res, 101(C10): 22737–22748, doi: 10.1029/96JC02123

Rogers R R, Yau M K. 1989. A Short Course in Cloud Physics. 3rd ed. New York: Pergamon Press

Sandven S, Johannesen O M. 2006. Sea ice monitoring by remote sensing. In: Gower J F R, ed. Manual of Remote Sensing: Remote Sensing of the Marine Environment. 3rd ed. Bethesda: American Society for Photogrammetry & Remote Sensing

Schröder D, Feltham D L, Flocco D, et al. 2014. September Arctic sea-ice minimum predicted by spring melt-pond fraction. Nat Climate Change, 4(5): 353–357, doi: 10.1038/nclimate2203

Semtner A J. 1976. A model for the thermodynamic growth of sea ice in numerical investigations of climate. J Phys Oceanogr, 6(3): 379–389

Skyllingstad E D, Paulson C A, Perovich D K. 2009. Simulation of melt pond evolution on level ice. J Geophys Res, 114(C12): C12019, doi: 10.1029/2009JC005363

Taylor P D. 2004. Mathematical modelling the formation and evolution of melt ponds on sea ice [dissertation]. London, UK: University of London

Taylor P D, Feltham D L. 2004. A model of melt pond evolution on sea ice. J Geophys Res, 109(C12): C12007, doi: 10.1029/2004JC002361

Untersteiner N. 1961. On the mass and heat budget of Arctic sea ice. Arch Meteor Geophys Bioklimatol Ser A, 12(2): 151–182

Weeks W F, Ackley S F. 1986. The growth, structure, and properties of sea ice. In: Untersteiner N, ed. The Geophysics of Sea Ice. New York, US: Springer, 9–164

Xie H, Lei R, Ke C, et al. 2013. Summer sea ice characteristics and morphology in the pacific Arctic sector as observed during the CHINARE 2010 cruise. Cryosphere, 7(4): 1057–1072

Yu Y, Rothrock D A. 1996. Thin ice thickness from satellite thermal imagery. J Geophys Res, 101(C11): 25753–25766

Zhang Shugang, Zhao Jinping, Shi Jiuxin, et al. 2014. Surface heat budget and solar radiation allocation at a melt pond during summer in the central Arctic Ocean. J Ocean Univ China, 13(1): 45–50